Article:
Luo, P., Yao, W. and Susmel, L. (2020) An improved critical plane and cycle counting method to assess damage under variable amplitude multiaxial fatigue loading. Fatigue and Fracture of Engineering Materials and Structures, 43 (9). pp. 2024-2039. ISSN: 8756-758X

https://doi.org/10.1111/ffe.13281

An improved critical-plane and cycle counting method to assess damage under variable amplitude multiaxial fatigue loading

Peng Luo[1*], Weixing Yao[1,2], Luca Susmel[3]

[1]*State Key Laboratory of Mechanics and Control of Mechanical Structures, Nanjing University of Aeronautics and Astronautics, Nanjing 210016, China*

[2]*Key Laboratory of Fundamental Science for National Defense-Advanced Design Technology of Flight Vehicle, Nanjing University of Aeronautics and Astronautics, Nanjing 210016, China*

[3]*Department of Civil and Structural Engineering, the University of Sheffield, Sheffield S1 3JD, UK*

Abstract: The plane with the maximum variance of the resolved shear stress is taken as the critical plane. Two algorithms are used along with the maximum variance method (MVM) to determine the orientation of the critical plane. The maximum variance of the normal stress on the potential critical planes is calculated to determine the one experiencing the maximum extent of fatigue damage. A new multiaxial cycle counting method is proposed to count cycles on the critical plane. The Modified Wöhler Curve Method is used to assess fatigue damage. About two hundred experimental results were collected from the technical literature to validate the approaches being proposed. The results show that the improved design technique being proposed is successful in assessing fatigue damage under variable amplitude multiaxial cyclic loading.

Keywords: multiaxial fatigue, variable amplitude, critical plane, maximum variance method

NOMENCLATURE

b	Fatigue strength exponent
b_0	Shear fatigue strength exponent
c	Fatigue ductility exponent
c_0	Shear fatigue ductility exponent
$C_{x,y}$	Covariance between signal x and y
E	Young's modulus
f	The ratio between the frequencies of the axial loading and torsional loading
G	Hessian matrix
m	Mean stress sensitivity index
R	Notch radius
S	Material constant
ρ	Loading non-proportionality factor
σ_{-1}	Fully reverse axial endurance limit
$\sigma_f^{'}$	Fatigue strength coefficient
$\sigma_{n,max}$	Maximum stress perpendicular to the critical plane
$\sigma_{n,m}$	Mean value of the stress normal to the critical plane.
σ_x	Normal stress component
$\varepsilon_f^{'}$	Fatigue ductility coefficient
$\Delta\varepsilon_n$	Range of the strain normal to the critical plane
τ_{-1}	Fully reverse torsional endurance limit
τ_a	The amplitude of shear stress relative to the critical plane
$\tau_f^{'}$	Shear fatigue strength coefficient
$\tau_q(t)$	Resolved shear stress on the critical plane
τ_{xy}	Shear stress component
$\gamma_f^{'}$	Shear fatigue ductility coefficient
γ_a	The amplitude of shear strain relative to the critical plane
$\Delta\gamma_{max}$	Range of shear strain on the critical plane

1 Introduction

Mechanical structures, such as aero engines and steam turbines, usually undergo multiaxial variable amplitude (VA) fatigue loading where the amplitude and mean value of the load history change with time[1-2]. For several decades, a large number of researchers worldwide have focused their attention on the development and validation of fatigue life analysis methods suitable for estimating damage under complex/multiaxial constant amplitude (CA) loading[3-6]. As a result, numerous approaches and theories have been proposed to estimate multiaxial fatigue lifetime, for instance, critical plane based methods[7-9], stress invariants based methods[10] and mesoscopic mechanical approaches[11]. Besides, attention has also been paid to predict the fatigue lifetime under multiaxial VA cyclic loading. Generally speaking, there are two strategies to assess fatigue lifetime under VA cyclic loading. The first one is the frequency domain method and the second is the time domain method[12-13]. In the first case, the Fourier transform is applied to obtain the stress power spectral density (PSD) function which is critical for the frequency domain method. The empirical models, such as Dirlik's model[14], Bendat's model[15] or Rice's model[16], are used to estimate the probability density function of the stress amplitude (PS). It should be noted that there is only one auto-power spectral density function under uniaxial VA fatigue loading while there are six auto-power spectral density functions and 30 cross-spectral density functions under multiaxial VA fatigue loading[17]. An equivalent PSD is usually adopted to estimate the PS under multiaxial VA fatigue loading. As for the time domain methods, there are three crucial elements for predicting the fatigue lifetime under complex VA cyclic loading[18]. The first one is to adopt a cycle counting method to discretize continuous load history into several loading cycles so that the peak and valley values of each loading cycle can be identified. The second one is to select a proper multiaxial fatigue damage parameter that can be used to evaluate the fatigue damage of each cycle. The third one is to quantify fatigue damage by employing a specific cumulative rule,

such as the linear damage cumulative rule (LDCR) proposed by Palmgren and Miner[19-20]. There are several kinds of uniaxial cycle counting methods as reviewed in Ref. [21]. A widely used method is the Rain-Flow cycle counting method (RCCM) which was firstly proposed by Matsuishi and Endo in 1968[22]. The physical basis of RCCM lies in the memory characteristic and the stress-strain hysteresis loop of metallic materials.

The entire loading history needs to be recorded before using the RCCM proposed by Matsuishi and Endo[22] because the loading history should be rearranged to reconstruct a new loading history which starts from the maximum stress. Downing *et al.*[23] reformulated the RCCM to be able to gather the real-time loading spectrum and count the associated loading cycles online. Moreover, the modified RCCM can reduce both memory consumption and computing time consumption.

At present, the cycle counting methods under uniaxial random loading are well established and widely used in a practical sense. In contrast, the cycle counting methods under multiaxial random fatigue loading are not yet well developed. There are two reasons that can explain this, and the first is that only one signal channel is used under uniaxial random loading, while at least two signal channels need to be managed simultaneously under multiaxial random fatigue loading. The second is that, as far as the critical plane concept is concerned, both the magnitude and direction of the shear stress on critical planes change periodically, which makes it more complicated to count cycles under multiaxial random fatigue loading.

Bannantine and Socie[24] combined the RCCM and the critical plane method to perform the cycle counting in terms of stresses and strains on the critical plane. However, this method can only be applied to post-process proportional VA load histories. Bannantine *et al.*[24] regarded the plane with the maximum fatigue damage as the critical plane by calculating the fatigue damage of all potential critical planes. The selected fatigue damage parameter depends on the failure

modes of materials. The SWT fatigue damage parameter[25] and the FS[7] fatigue damage parameter are respectively used for Mode I and Mode II dominated crack initiation. The two fatigue damage parameters can be expressed as follows:

$$\begin{aligned} &\text{SWT}: \frac{\Delta\varepsilon_{\mathrm{n}}}{2}\sigma_{\mathrm{n,max}} = \frac{\sigma_{\mathrm{f}}^{'}}{E}\left(2N_{\mathrm{f}}\right)^{2b} + \sigma_{\mathrm{f}}^{'}\varepsilon_{\mathrm{f}}^{'}\left(2N_{\mathrm{f}}\right)^{b+c} \\ &\text{FS}: \ \gamma_{\mathrm{a}}\left(1+\frac{\sigma_{\mathrm{n}}}{\sigma_{\mathrm{y}}}\right) = \gamma_{\mathrm{f}}^{'}\left(2N_{\mathrm{f}}\right)^{c_0} + \frac{\tau_{\mathrm{f}}^{'}}{G}\left(2N_{\mathrm{f}}\right)^{b_0} \end{aligned} \tag{1}$$

where $\triangle\varepsilon_{\mathrm{n}}$ and $\sigma_{\mathrm{n,\,max}}$ are respectively the range of normal strain and the maximum normal stress on the critical plane. γ_{a} is the amplitude of shear strain on the critical plane. $\sigma_{\mathrm{f}}^{'}$ and $\varepsilon_{\mathrm{f}}^{'}$ are respectively fatigue strength coefficient and fatigue ductility coefficient, $\tau_{\mathrm{f}}^{'}$ and $\gamma_{\mathrm{f}}^{'}$ are respectively shear fatigue strength coefficient and shear fatigue ductility coefficient. b and c are respectively fatigue strength exponent and fatigue ductility exponent, b_0 and c_0 are respectively shear fatigue strength exponent and shear fatigue ductility exponent.

Wang and Brown[26-28] proposed a cycle counting method for non-proportional VA fatigue loading. The relative value of the Von-Mises strain is taken as the counting parameter. Besides, to consider the influence of non-proportional loading, they[26] proposed a fatigue damage parameter under non-proportional cyclic loading. They assumed that fatigue damage is only related to the value of the normal stress between adjacent turning points of the shear strain on the critical plane, but their relative position is assumed to be unimportant. Once the maximum shear strain changes its direction, the history effect of the normal strain is erased. Therefore, the normal stress range between adjacent turning points of the shear strain and the amplitude of shear strain is used to define the well-known Wang and Brown's fatigue damage parameter:

$$\frac{0.5\Delta\gamma_{\mathrm{max}} + S\Delta\varepsilon_{\mathrm{n}}^{*}}{1+\upsilon'+(1-\upsilon')S} = \frac{\sigma_{\mathrm{f}}^{'}\text{-}2\sigma_{\mathrm{n,m}}}{E}\left(2N_{\mathrm{f}}\right)^{b} + \varepsilon_{\mathrm{f}}^{'}\left(2N_{\mathrm{f}}\right)^{c} \tag{2}$$

where $\Delta\gamma_{\mathrm{max}}$ is the range of shear strain on the critical plane, S is a material fatigue constant, $\sigma_{\mathrm{n,m}}$ is the mean value of stress normal to the critical plane, and υ' is the effective Poisson's

ratio which can be determined according to the deformation theory.

Since the direction of the normal stress on the critical plane is fixed, Carpinteri *et al.*[29] defined the normal stress on the critical plane as the main channel and the shear stress on the critical plane as the auxiliary channel. Carpinteri *et al.*[29] assumed that there is a deflection angle δ[30] between the critical plane and the weighted average direction of the maximum principal stress. The angle δ[30] is expressed as:

$$\delta=45\cdot\frac{3}{2}\left[1-\left(\frac{\tau_{-1}}{\sigma_{-1}}\right)^{2}\right] \tag{3}$$

where σ_{-1} and τ_{-1} are the fully reverse axial fatigue limit and the torsional fatigue limit, respectively.

Langlais *et al.*[31] proposed a multiaxial rainflow algorithm which makes a slight modification of the uniaxial standards. The recorded loading point could be discarded during the counting procedure for two reasons: 1) when the newest point defines a new peak in the same direction as the previous or 2) when a cycle is finished. Dong *et al.*[32] proposed a Path-Dependent Maximum Range (PDMR) for performing fatigue evaluation of engineering components under variable-amplitude and arbitrary multi-axial conditions, which can recover conventional rainflow cycle counting results exactly under uniaxial conditions. Anes *et al.*[33] implemented the Stress Scale Factor (SSF) virtual cycle counting method based on the SSF equivalent shear stress early proposed by Anes *et al.*[34]. Portugal *et al.*[35] conducted a cycle counting method to predict the VA fatigue life of Rolling Contact Fatigue (RCF), which includes two channels, one is the maximum value of the normal stress vector during the entire loading history and the other is the shear stress based on the minimum circumscribed circle approach[36]. Wang *et al.*[37] proposed two multiaxial cycle counting methods based on the RCCM and range cycle counting methods for uniaxial loading. The critical plane is determined by a weight function method[37]. Lu *et al.*[38] applied the energy-based fatigue damage parameter to assess the low-cycle fatigue damage under random

VA loading. The idea to assess the VA fatigue damage is to divide the irregular loading path into several regular loading paths[38].

Susmel *et al.*[18,39-42] defined the plane experiencing the maximum variance of the resolved shear stress as the critical plane, where the RCCM can be easily used to count the cycles since the resolved shear stress is a one-dimensional stress quantity. Both the stress-based MVM[39] and the strain-based MVM[42] were proposed and checked against a large number of experimental results coming from testing plain and notched specimens under multiaxial VA fatigue loading.

In this paper, two types of algorithms (Newton method and conjugate gradient method) are used to implement the maximum variance method (MVM) and improve the original numerical solution proposed in Ref [43]. The maximum variance of normal stress is proposed to select, amongst all the potential critical planes, the material plane experiencing the maximum fatigue damage. A new multiaxial cycle counting method is then formulated by taking the resolved shear stress on the critical plane as the main channel and the normal stress on the critical plane as the auxiliary channel. Finally, the accuracy and reliability of these improved design approaches were checked against a large number of experimental data collected from literature.

2 The modified MVM

2.1 Introduction of MVM to determine the critical plane

The variance is an important concept in mathematical statistics[44-46]. Consider two periodic signals, x(t) and y(t), that change over time. The mean value of signal $x(t)$ is defined as follows:

$$E(x) = \frac{1}{T}\int_0^T x(t)dt \tag{4}$$

The variance of the periodic signal x(t) is defined as follows:

$$V(x) = E\left\{\left[x(t)-E(x)\right]^2\right\} = \frac{1}{T}\int_0^T \left[x(t)-E(x)\right]^2 dt \tag{5}$$

The equivalent amplitude of the periodic sinusoidal signal x(t) can be calculated as follows:

$$x_a = \sqrt{2V(x)} \tag{6}$$

The covariance between x(t) and y(t) is:

$$C_{x,y} = E\left\{\left[x(t)-E(x)\right]\cdot\left[y(t)-E(y)\right]\right\} = \frac{1}{T}\int_0^T \left\{\left[x(t)-E(x)\right]\cdot\left[y(t)-E(y)\right]\right\}dt \tag{7}$$

The variance is used to characterize the dispersion of random signals. A small variance means that the data of a random signal is highly centralized in respect to the mean value.

The fatigue damage is closely related with the variance of stress under uniaxial cyclic loading. For complex cyclic loading history, Susmel[40,43] assumed that the critical plane is the plane experiencing the maximum variance of the resolved shear stress. Consider a point O under complex random cyclic loading. The stress tensor of point O is σ_{ij}(t). The global coordinate system O-*xyz* is shown in Figure1 (*a*). An arbitrary plane $\triangle$ with normal unit vector $\boldsymbol{n}$ passes through the point O. A new local right-hand coordinate system O-*abn* could be defined if the axis $\boldsymbol{a}$ lies in the plane *O-xy*. The definition of angle θ and ϕ is shown in Figure1 (*a*). The unit vectors of the coordinate system O-*abn* can be expressed as follows:

$$\boldsymbol{n} = \begin{bmatrix} n_x \\ n_y \\ n_z \end{bmatrix} = \begin{bmatrix} \sin\theta\cos\phi \\ \sin\theta\sin\phi \\ \cos\theta \end{bmatrix} \quad \boldsymbol{a} = \begin{bmatrix} a_x \\ a_y \\ a_z \end{bmatrix} = \begin{bmatrix} \sin\phi \\ -\cos\phi \\ 0 \end{bmatrix} \quad \boldsymbol{b} = \begin{bmatrix} b_x \\ b_y \\ b_z \end{bmatrix} = \begin{bmatrix} \cos\theta\cos\phi \\ \cos\theta\sin\phi \\ -\sin\theta \end{bmatrix} \tag{8}$$

An arbitrary direction $\boldsymbol{q}$ lies on the plane $\triangle$ and passes through the point O in Figure1 (*b*). The angle between direction $\boldsymbol{q}$ and axis $\boldsymbol{a}$ is defined as α. The unit vector $\boldsymbol{q}$ is:

$$\boldsymbol{q} = \begin{bmatrix} q_x \\ q_y \\ q_z \end{bmatrix} = \begin{bmatrix} \cos\alpha\sin\phi + \sin\alpha\cos\theta\cos\phi \\ -\cos\alpha\cos\phi + \sin\alpha\cos\theta\sin\phi \\ -\sin\alpha\sin\theta \end{bmatrix} \tag{9}$$

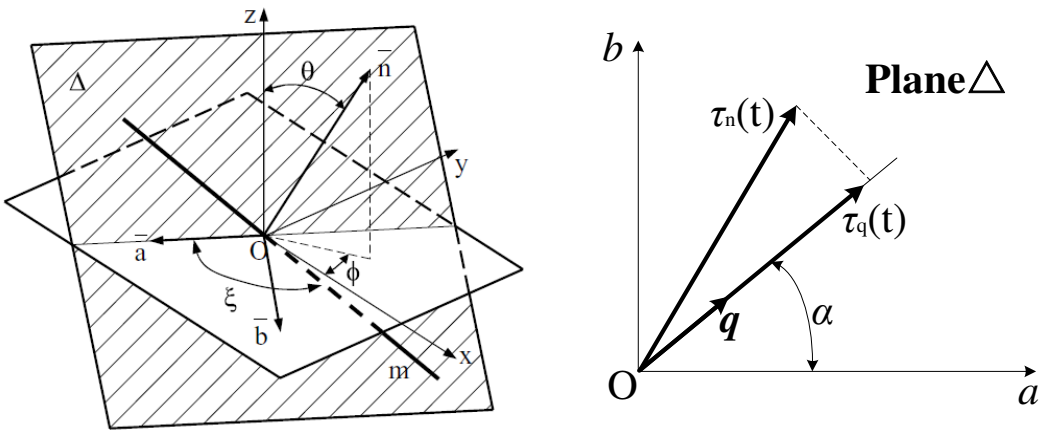

(*a*) (*b*)

Figure 1 The illustration of global coordinate system O-*xyz* and local coordinate system O-*abn*

The normal stress $\sigma_{\mathrm{n}}(\mathrm{t})$ and the resolved shear stress $\tau_{\mathrm{q}}(\mathrm{t})$ along the direction $\boldsymbol{q}$ on the plane △ are expressed as:

$$\sigma_{\mathrm{n}}(\mathrm{t})=\boldsymbol{n}^{\mathrm{T}}\cdot\boldsymbol{\sigma}_{\mathrm{ij}}(t)\cdot\boldsymbol{n}=\begin{bmatrix}n_x & n_y & n_z\end{bmatrix}\begin{bmatrix}\sigma_x & \tau_{xy} & \tau_{xz}\\ \tau_{xy} & \sigma_y & \tau_{yz}\\ \tau_{xz} & \tau_{yz} & \sigma_z\end{bmatrix}\begin{bmatrix}n_x\\ n_y\\ n_z\end{bmatrix}=\boldsymbol{d}\cdot\boldsymbol{s}(\mathrm{t}) \tag{10}$$

$$\tau_{\mathrm{q}}(\mathrm{t})=\boldsymbol{q}^{\mathrm{T}}\cdot\boldsymbol{\sigma}_{\mathrm{ij}}(t)\cdot\boldsymbol{n}=\begin{bmatrix}q_x & q_y & q_z\end{bmatrix}\begin{bmatrix}\sigma_x & \tau_{xy} & \tau_{xz}\\ \tau_{xy} & \sigma_y & \tau_{yz}\\ \tau_{xz} & \tau_{yz} & \sigma_z\end{bmatrix}\begin{bmatrix}n_x\\ n_y\\ n_z\end{bmatrix}=\boldsymbol{D}\cdot\boldsymbol{s}(\mathrm{t}) \tag{11}$$

where,

$$\boldsymbol{d}=\begin{bmatrix}d_1\\ d_2\\ d_3\\ d_4\\ d_5\\ d_6\end{bmatrix}^{\mathrm{T}}=\begin{bmatrix}n_x^2\\ n_y^2\\ n_z^2\\ 2n_xn_y\\ 2n_xn_z\\ 2n_yn_z\end{bmatrix}^{\mathrm{T}}=\begin{bmatrix}\sin^2\theta\cos^2\phi\\ \sin^2\theta\sin^2\phi\\ \cos^2\theta\\ 2\sin^2\theta\sin\phi\cos\phi\\ 2\sin\theta\cos\theta\cos\phi\\ 2\sin\theta\cos\theta\sin\phi\end{bmatrix}^{\mathrm{T}} \tag{12}$$

$$\boldsymbol{D}=\begin{bmatrix}D_1\\ D_2\\ D_3\\ D_4\\ D_5\\ D_6\end{bmatrix}^{\mathrm{T}}=\begin{bmatrix}n_xq_x\\ n_yq_y\\ n_zq_z\\ n_xq_y+n_yq_x\\ n_xq_z+n_zq_x\\ n_yq_z+n_zq_y\end{bmatrix}^{\mathrm{T}}=\begin{bmatrix}\frac{1}{2}\left(\sin\theta\sin2\phi\cos\alpha+\sin\alpha\sin2\theta\cos^2\phi\right)\\ \frac{1}{2}\left(-\sin\theta\sin2\phi\cos\alpha+\sin\alpha\sin2\theta\sin^2\phi\right)\\ -\frac{1}{2}\sin\alpha\sin2\theta\\ \frac{1}{2}\sin\alpha\sin2\phi\sin2\theta-\cos\alpha\cos2\phi\sin\theta\\ \sin\alpha\cos\phi\cos2\theta+\cos\alpha\sin\phi\cos\theta\\ \sin\alpha\sin\phi\cos2\theta-\cos\alpha\cos\phi\cos\theta\end{bmatrix}^{\mathrm{T}} \tag{13}$$

$$\boldsymbol{s}(t)=\begin{bmatrix} s_1 \\ s_2 \\ s_3 \\ s_4 \\ s_5 \\ s_6 \end{bmatrix}=\begin{bmatrix} \sigma_x(t) \\ \sigma_y(t) \\ \sigma_z(t) \\ \sigma_{xy}(t) \\ \sigma_{xz}(t) \\ \sigma_{yz}(t) \end{bmatrix} \tag{14}$$

According to the definition in Eq. (5), the variance of the resolved shear stress $\tau_{\mathrm{q}}(\mathrm{t})$ is:

$$\begin{aligned} \mathrm{Var}\left[\tau_q(t)\right] &= \mathrm{Var}\left[\boldsymbol{D}\cdot\boldsymbol{s}(t)\right]=\mathrm{Var}\left[\sum_{k=1}^{6}\left(D_k\cdot s_k\right)\right] \\ &=\sum_{k=1}^{6}\left\{D_k^2\cdot\mathrm{Var}\left[s_k\right]\right\}=\boldsymbol{D}\cdot\mathrm{Var}\left[\boldsymbol{s}\right]\cdot\boldsymbol{D}^{\mathrm{T}} \\ &=\boldsymbol{D}\cdot\boldsymbol{C}\cdot\boldsymbol{D}^{\mathrm{T}} \end{aligned} \tag{15}$$

where $\boldsymbol{C}$ is the covariance matrix of matrix $\boldsymbol{s}$ which is shown as follows:

$$\boldsymbol{C}=\begin{bmatrix} V_x & C_{x,y} & C_{x,\mathrm{z}} & C_{x,xy} & C_{x,xz} & C_{x,yz} \\ C_{x,y} & V_y & C_{y,\mathrm{z}} & C_{y,xy} & C_{y,xz} & C_{y,yz} \\ C_{x,z} & C_{y,\mathrm{z}} & V_z & C_{z,xy} & C_{z,xz} & C_{z,yz} \\ C_{x,xy} & C_{y,xy} & C_{z,xy} & V_{xy} & C_{xy,xz} & C_{xy,yz} \\ C_{x,xz} & C_{y,xz} & C_{z,xz} & C_{xy,xz} & V_{xz} & C_{xz,yz} \\ C_{x,yz} & C_{y,yz} & C_{z,yz} & C_{xy,yz} & C_{xz,yz} & V_{yz} \end{bmatrix} \tag{16}$$

where $V_i=\frac{1}{T}\int_0^T\left[\sigma_i(t)-E(\sigma_i)\right]^2dt$ and $C_{i,j}=\frac{1}{T}\int_0^T\left\{\left[\sigma_i(t)-E(\sigma_i)\right]\cdot\left[\sigma_j(t)-E(\sigma_j)\right]\right\}dt$. More details and derivation process of $\mathrm{Var}\left[\tau_q(t)\right]$ can be found in Ref [43].

2.2 The MVM of normal stress on the critical plane

How to select the critical plane from several potential planes bearing the global maximum variance of resolved shear stress? The idea is to construct the variance of normal stress on these potential planes, like the variance of the resolved shear stress. The variance of signals is positively correlated with the amplitude of signals according to the definition in Eq. (6). The variance of normal stress is expressed as:

$$\begin{aligned} \mathrm{Var}\left[\sigma_{\mathrm{n}}(t)\right] &= \mathrm{Var}\left[\boldsymbol{d}\cdot\boldsymbol{s}(\mathrm{t})\right]=\mathrm{Var}\left[\sum_{k=1}^{6}\left(d_k\cdot s_k\right)\right] \\ &=\sum_{k=1}^{6}\left\{d_k^2\cdot\mathrm{Var}\left[s_k\right]\right\}=\boldsymbol{d}\cdot\mathrm{Var}\left[\boldsymbol{s}\right]\cdot\boldsymbol{d}^{\mathrm{T}} \\ &=\boldsymbol{d}\cdot\boldsymbol{C}\cdot\boldsymbol{d}^{\mathrm{T}} \end{aligned} \tag{17}$$

The mean value of normal stress $\sigma_{\mathrm{n,m}}$ is defined as follows:

$$\begin{aligned}\sigma_{\mathrm{n,m}} &= \frac{1}{T}\int_0^T \sigma_n(t)\,dt = \frac{1}{T}\int_0^T [\boldsymbol{d}\cdot\boldsymbol{s}(\mathrm{t})]dt \\ &= \frac{1}{T}\int_0^T \left[\sum_{i=1}^{6} d_i s_i(t)\right]dt = \sum_{i=1}^{6}\left[d_i\left(\frac{1}{T}\int_0^T s_i(t)dt\right)\right] \\ &= \sum_{i=1}^{6}\left(d_i s_{i,m}\right) = \boldsymbol{d}\cdot\boldsymbol{s}_m\end{aligned} \tag{18}$$

where,

$$\boldsymbol{s}_{\mathrm{m}} = \begin{bmatrix} s_{1,\mathrm{m}} \\ s_{2,\mathrm{m}} \\ s_{3,\mathrm{m}} \\ s_{4,\mathrm{m}} \\ s_{5,\mathrm{m}} \\ s_{6,\mathrm{m}} \end{bmatrix} = \begin{bmatrix} \sigma_{x,\mathrm{m}} \\ \sigma_{y,\mathrm{m}} \\ \sigma_{z,\mathrm{m}} \\ \sigma_{xy,\mathrm{m}} \\ \sigma_{xz,\mathrm{m}} \\ \sigma_{z,\mathrm{m}} \end{bmatrix} \tag{19}$$

where $\sigma_{i,\mathrm{m}}$ is the stress mean value of the stress component σ_i.

According to Eq. (6), Eq. (18)-(19), the maximum stress on the planes can be expressed as:

$$\sigma_{n,\max} = \sigma_a + \sigma_{n,\mathrm{m}} = \sqrt{2\left(\boldsymbol{d}\cdot\boldsymbol{C}\cdot\boldsymbol{d}^{\mathrm{T}}\right)} + \boldsymbol{d}\cdot\boldsymbol{s}_m \tag{20}$$

In order to determine the critical plane, the maximum normal stresses need to be calculated on these potential planes. The potential plane with the maximum normal stresses is the critical plane.

It is worth noting that the covariance matrix $\boldsymbol{C}$ in Eq. (15) only depends on the loading history and can be regarded as a constant matrix to search the plane with the maximum variance of resolved shear stress. The key to determine the critical plane with the maximum variance of the resolved shear stress $\tau_{\mathrm{q}}(\mathrm{t})$ is to search the maximum value of Eq. (15). A so-called gradient ascent method was used in Ref. [43] to find the maximum value of Eq. (15), but the iterative step of the algorithm in Ref. [43] is constant which makes the calculation time-consuming and the iteration hard to reach convergence. Two kinds of advanced gradient ascent methods are used to modify the algorithm proposed in Ref. [43]. One is the Newton method[47] and the other is the conjugate gradient method[48], which are introduced in detail in Appendix 1.

3 A new multiaxial cycle counting method

It is necessary to consider at least two channels in the cycle counting method under multiaxial fatigue loading. It has been proven that the critical plane approach is an effective and useful theory to evaluate the fatigue life under complex cyclic loading[31,40,49,50]. Therefore, it is reasonable to regard the normal stress and the shear stress on the critical plane as two channels in the multiaxial cycle counting. The normal stress is a one-dimensional vector whose direction is perpendicular to the critical plane. However, the shear stress is a two-dimensional vector that rotates on the critical plane. The value and direction of the shear stress on the critical plane change during complex cyclic loading. It is easy to count the normal stress on the critical plane while it is difficult to count the shear stress on the critical plane. It is worth noting that the resolved shear stress is a one-dimensional vector in Figure 1(b)[43,40]. Therefore, it is very convenient to regard the normal stress and the resolved shear stress on the critical plane as two channels to count the multiaxial VA fatigue loading. Besides, the shear stress is the driving force of crack initiation. It is reasonable to regard the resolved shear stress on the critical plane as the main channel and take the normal stress on the critical plane as the auxiliary channel in the multiaxial cycle counting.

Luo *et al.*[4] collected a large number of experimental data to evaluate the accuracy and applicability of different multiaxial fatigue damage parameters. The results showed that the Susmel's multiaxial fatigue parameter[51-53] based on the critical plane theory is the best to assess the fatigue life under multiaxial cyclic loading. Susmel's parameter is:

$$\tau_{\mathrm{eq}} = \tau_a + \left(\tau_{-1} - \sigma_{-1}/2\right)\rho \tag{21}$$

$$\rho = \left[\min\left(\rho_0, \rho_{\lim}\right)\right] \tag{22}$$

$$\rho_0 = \frac{\sigma_{\mathrm{n,max}}}{\tau_a} = \frac{\sigma_{\mathrm{n},a} + m\sigma_{\mathrm{n},m}}{\tau_a} \tag{23}$$

$$\rho_{\lim} = \frac{\tau_{-1}}{2\tau_{-1} - \sigma_{-1}} \tag{24}$$

where σ_{-1} and τ_{-1} are fully reversed uniaxial fatigue limit and fully reversed torsional fatigue limit, respectively. m is the mean stress sensitivity index which can be determined by test. τ_a and $\sigma_{n,max}$ are the amplitude of shear stress and the maximum normal stress on the critical plane, respectively.

According to the test in Ref. [22]–[24] and Ref. [54], only the normal stress contribution between the cycles of the maximum shear stress is effective to enhance fatigue crack initiation. Once the cycle of the maximum resolved shear stress is different, the effect of the normal stress disappears. Besides, the relative position of the excursion of the normal stress between the cycles of the resolved shear stress can not affect fatigue damage.

The process of this new multiaxial cycle counting method is shown in Figure 2 where the critical plane is determined through the MVM of resolved shear stress and the MVM of normal stress. The resolved shear stress history and normal stress history on the critical plane could be regarded as two channels to count the multiaxial VA fatigue loading, and the resolved shear stress is the main channel. Firstly, the resolved shear stress on the critical plane is counted according the modified RCCM proposed by Dong *et al.*[32]. The amplitude and the cycles of the resolved shear stress are recorded. Then, the excursion of the normal stress between the cycles of the resolved shear stress is recorded. The amplitude of resolved shear stress and the maximum normal stress on the critical plane are the main parameters in Susmel's multiaxial fatigue damage parameter according the Eq. (21-24) which can be used to assess the fatigue damage of each cycle.

An example is listed to further explain the new cycle counting method in Figure 3. The first step is to calculate the stress components on the critical plane by MVM. S1 in Figure 3(*a*) is the original stress history of normal stress and resolved shear stress on the critical plane. The second step is to discard the points which are not the peak or the valley for both channels, like the point

9 in Figure 3(*b*). The third step is to take the resolved shear stress as the main channel and count the cycles of the resolved shear stress by RCCM. Then, get the maximum normal stress between the counted cycles of the resolved shear stress in Figure 3(*c*). The fourth step is to discard the points of resolved shear stress which has been counted and remain all the normal stress history on the critical plane. Repeat the third step until all the cycles of the resolved shear stress are counted, like in Figure 3(*d*).

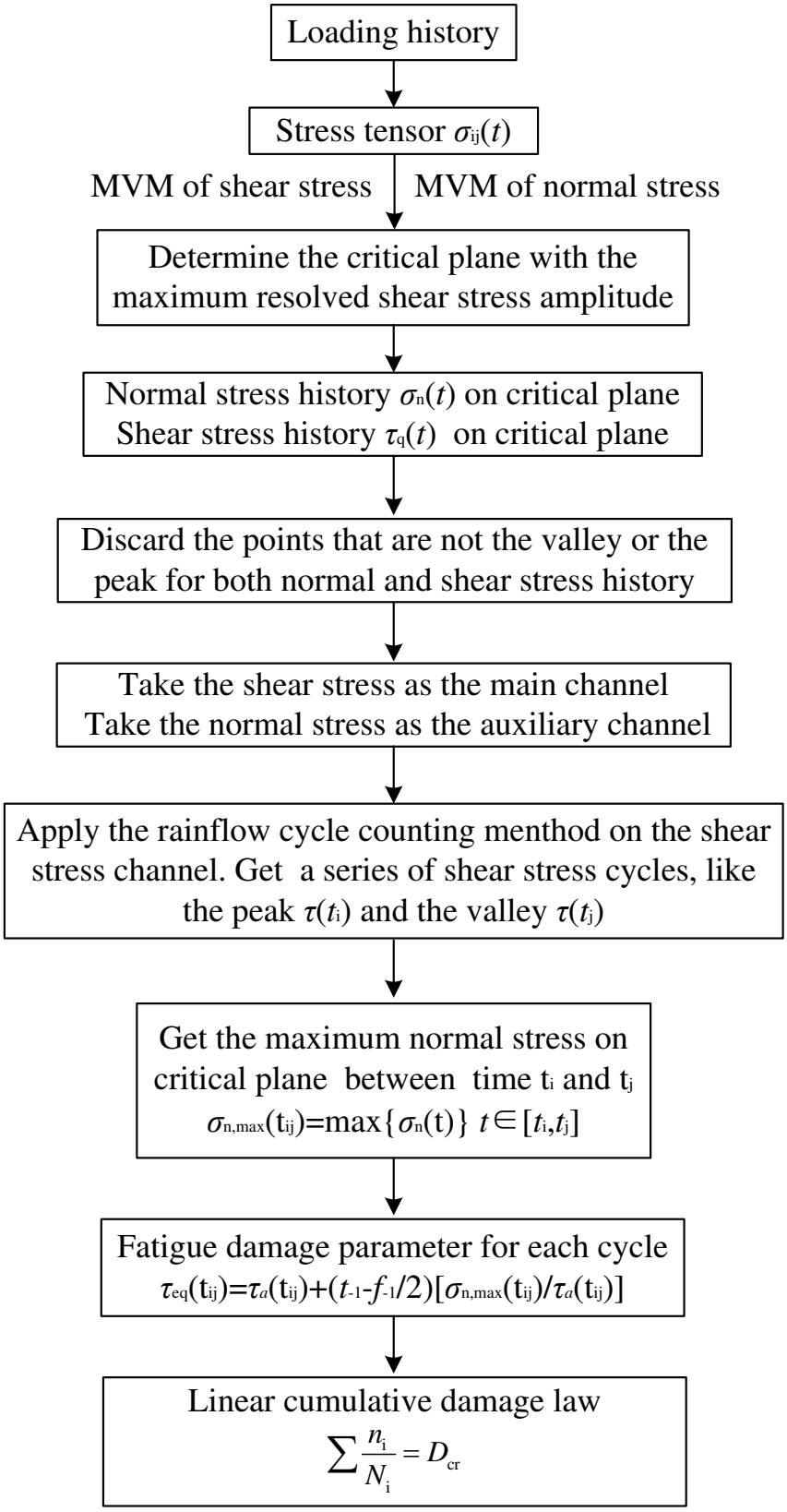

Figure 2 The process of the new multiaxial cycle counting method

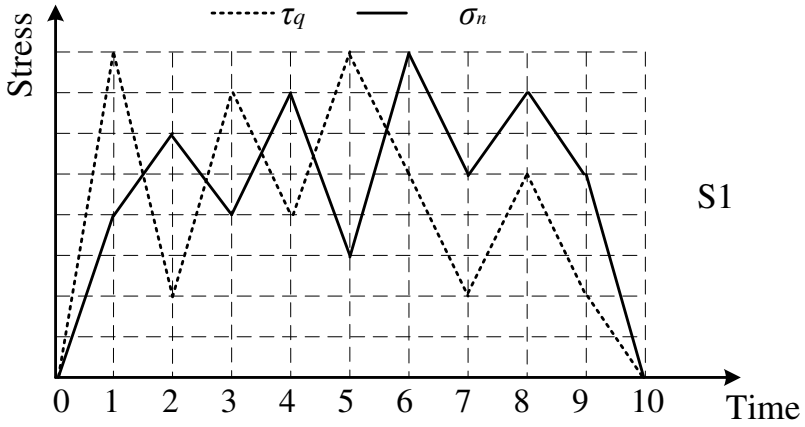

(*a*) Original normal stress and resolved shear stress history on the critical plane

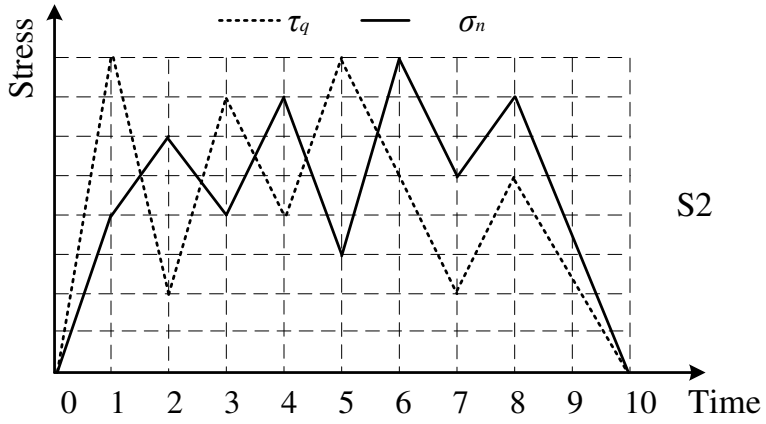

(*b*) Discard the point 9 which is not the peak or valley for both resolved shear stress and normal stress

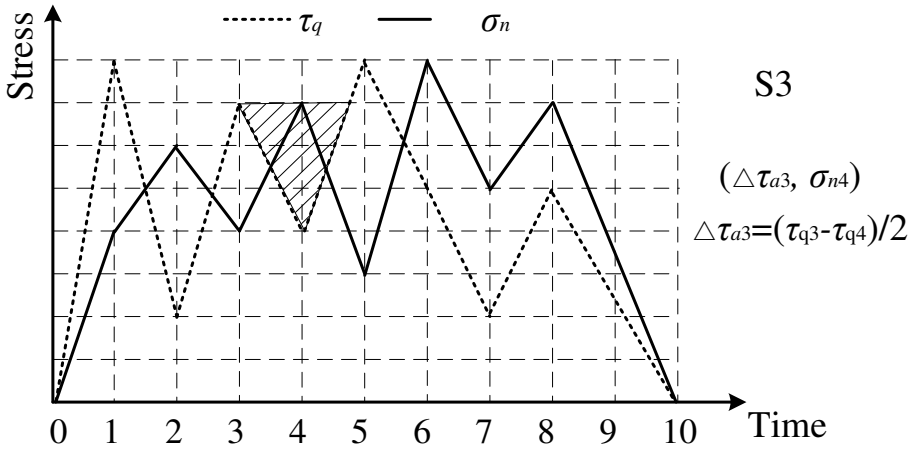

(*c*) Apply the rainflow cycle counting method to count the resolved shear stress cycle and get the maximum normal stress between the two points of the resolved shear stress

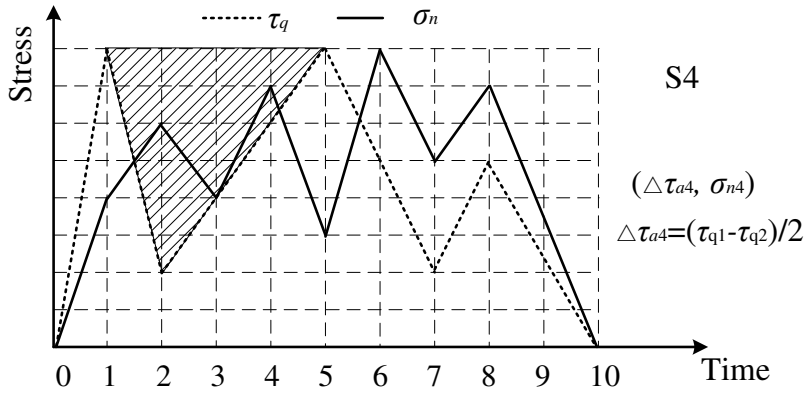

(*d*) Discard the point 2 and point 3 of the resolved shear stress and remain all the loading history of normal stress. Then repeat S3

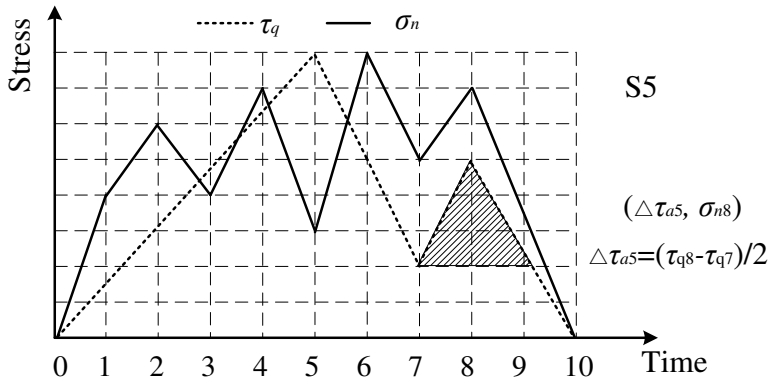

(*e*) Repeat S4 until all the cycles of resolved shear stress are counted.

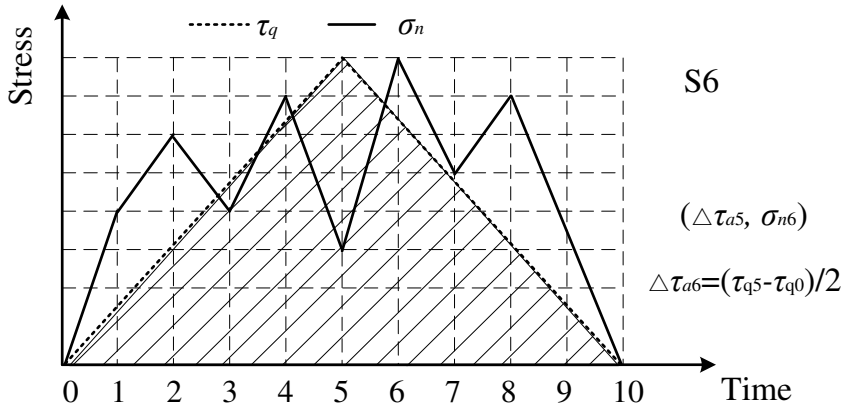

(*f*) Repeat S5 until all the cycles of resolved shear stress are counted.

Figure 3 An example of the new multiaxial cycle counting method

4 Experimental data collection and model verification

4.1 Experimental data collection

The complex variable amplitude fatigue test data for six different kinds of metallic materials are collected to verify the new method. The mechanical properties and the fatigue properties of

these materials are summarized in Table 1. It should be noted that the specimens made of 2020-T4[55], XC18[56] and 39NiCrMo3[57] are smooth while the specimens made of C40[39], TC4[58] and En8[42] are notched specimens. The shape of the smooth specimens is cylindrical. The dimensions of the notched specimens are shown in Figure 4. The experimental multiaxial VA loading history of these materials is reported in Appendix 2. More details about these fatigue tests are introduced in the literature.

The fatigue life of multiaxial notches can be evaluated by combining the fatigue strength reduction factor K_f with the multiaxial nominal stress, which was proposed by Lazzarin and Susmel in 2003[52]. Lazzarin and Susmel[52] assumed that there is a linear relation between the multiaxial fatigue strength reduction factor K_f and the loading non-proportionality factor ρ defined in Eq. (23). The predicted lives using K_f and ρ are in good agreement with experimental lives for notched specimens under multiaxial cyclic loading. The linear relation is expressed as follows:

$$K_f(\rho) = a_1\rho + b_1 \tag{25}$$

where ρ is the loading non-proportionality factor which can represent the degree of non-proportionality for multiaxial loading. ρ equals to one for uniaxial fatigue loading and ρ equals to zero for torsional fatigue loading. Parameters a_1 and b_1 can be calculated by testing two notched specimens under reversed uniaxial fatigue loading and reversed torsional fatigue loading respectively. Assuming that the fatigue strength reduction factor is K_{f1} under reversed uniaxial fatigue loading and fatigue strength reduction factor is K_{f2} under reversed torsional fatigue loading. The expressions of parameters a_1 and b_1 in Eq.(25) are deduced:

$$\begin{aligned} a_1 &= K_{f1} - K_{f2} \\ b_1 &= K_{f2} \end{aligned} \tag{26}$$

The parameters a_1 and b_1 in Eq. (25) for six materials are listed in Table 2.

Table 1 The mechanical properties and the fatigue properties of metallic materials

Materials	E/GPa	σ_b/MPa	σ_{-1}/MPa	τ_{-1}/MPa	m
2020-T4[55]	73	545	168.0	120.0	***
XC18[56]	210	520	310.0	179.0	***
39NiCrMo3[57,59]	206	856	367.5	265.0	***
C40[39]	209	850	292.8	231.7	0.19
TC4[58]	108.4	945.2	248.3	192.4	***
En8[42]	210	701	223.3	179.6	0.24

Note: *** means that the fatigue loading is symmetrical.

Table 2 The parameters a_1 and b_1

Materials	Notch radius R/mm	a_1	b_1
C40[39]	0.225	0.83	1.76
	1.2	0.71	1.52
	3	0.46	1.39
TC4[58]	1	0.59	1.81
En8[42]	1.5	0.66	1.61
	3	0.47	1.45
	6	0.26	1.36

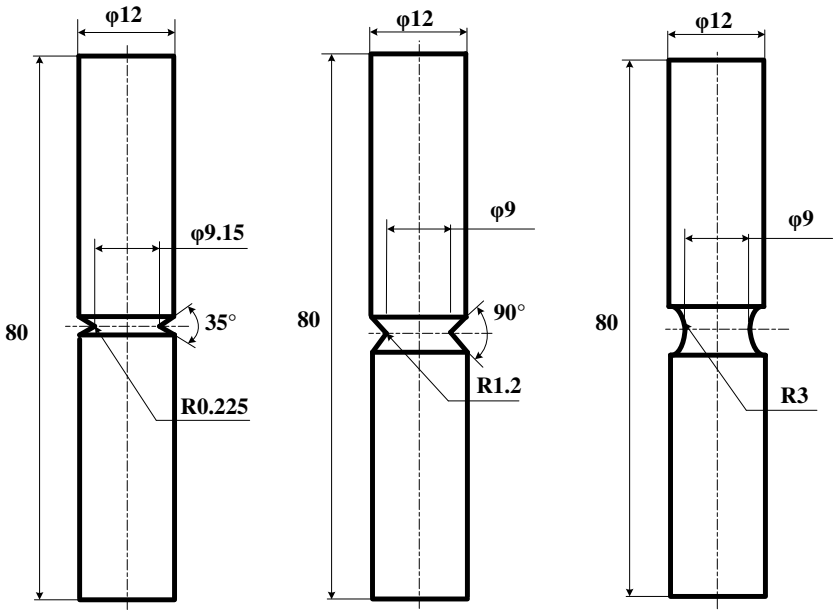

(*a*) The notched specimens made of C40[39]

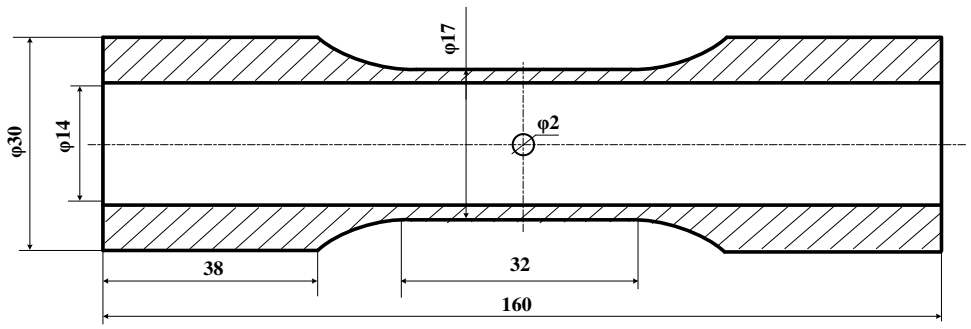

(*b*) The notched specimens made of TC4[58]

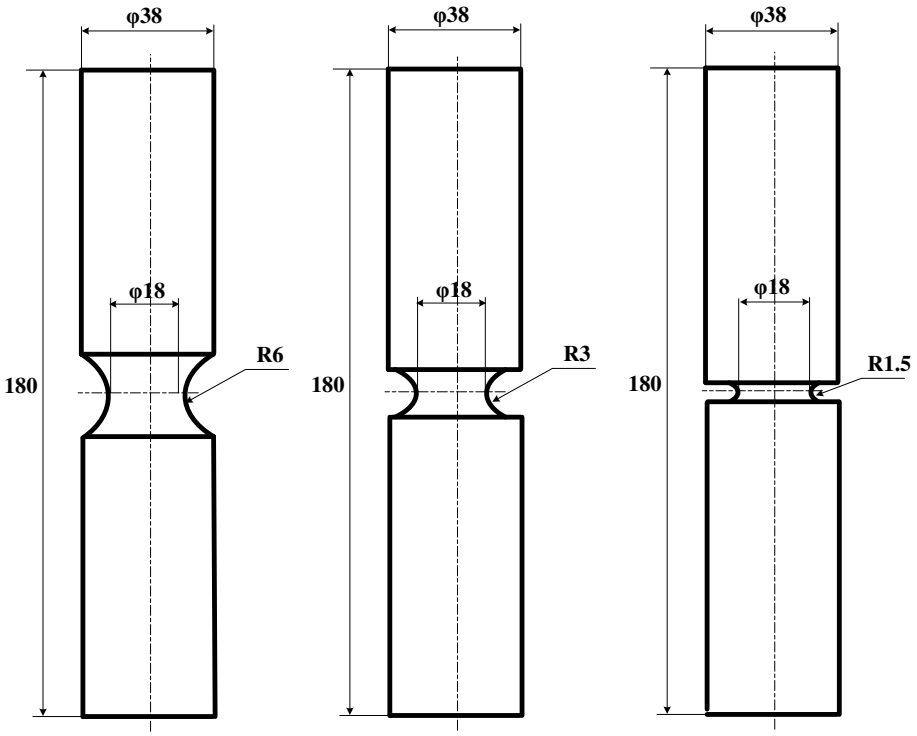

(*c*) The notched specimens made of En8[42]

Figure 4 The dimensions of notched specimens

4.2 Model verification

The Modified MVM of the resolved shear stress and the normal stress are used to determine the direction of the critical plane for both plain and notched specimens under complex variable amplitude cyclic loading. Then, the new multiaxial cycle counting method is applied to count the values of Susmel's multiaxial damage parameter. In the end, the sum of all the fatigue damage is cumulated by Miner's LDCR. The range of critical damage D_{cr} is from 0.02 to 5 which can be accurately determined by a large number of fatigue experiments. Sonsino *et al.*[60-62] suggest the

D_{cr} is 0.37 for aluminum and 0.27 for steel to ensure the safety of the designed structure. The comparison between experimental life and predicted life for plain specimens is shown in Figure 5. The comparison between experimental life and predicted life for notched specimens is shown in Figure 6. Most of the predicted lives of plain specimens fall within 2-time error band and all the predicted lives of plain specimens fall within 4-time error band. The predicted lives of notched specimens are more dispersed than that of smooth specimens due to the limitation of the nominal stress approach. Nevertheless, most of the predicted lives of notched specimens fall within 4-time error band according to Figure 6. It should be noted that the f in Figure 6 (h) represents the ratio between the frequencies of the axial loading and torsional loading.

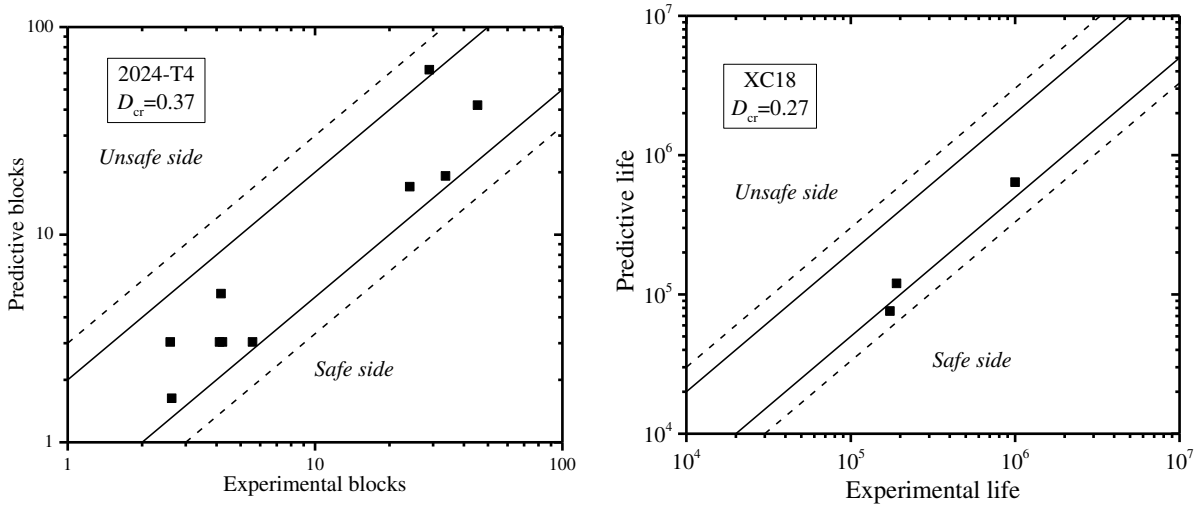

(a) (b)

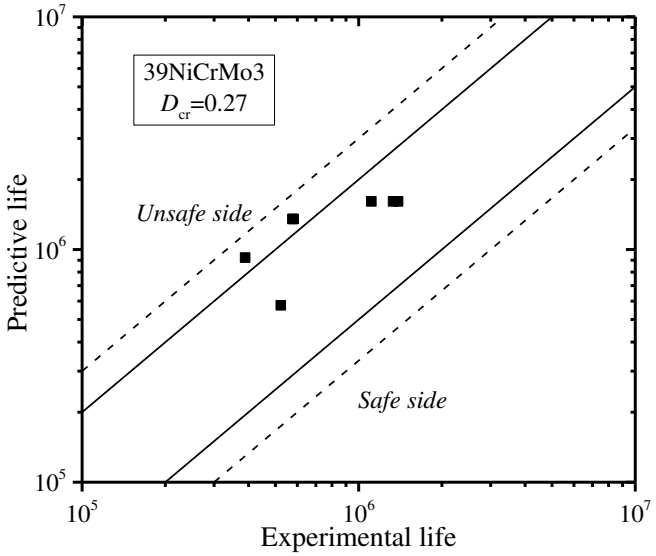

(*c*)

Figure 5 The comparison between experimental life and predicted life for plain specimens

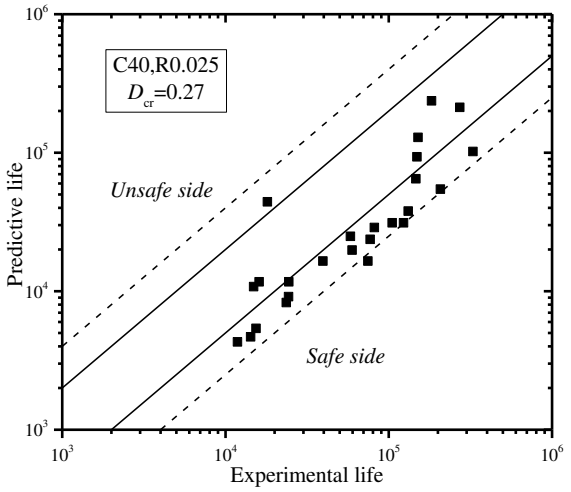

(*a*)

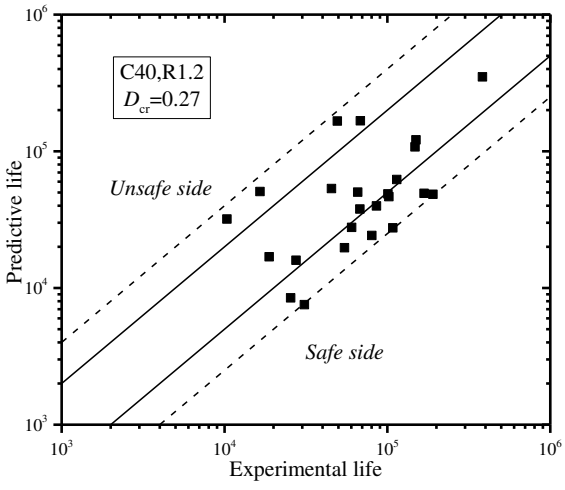

(*b*)

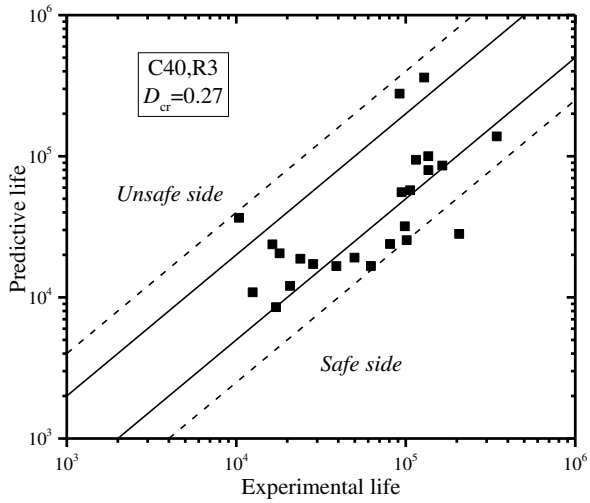
C40,R3
D_{cr}=0.27
Unsafe side
Safe side
Predictive life
Experimental life

(*c*)

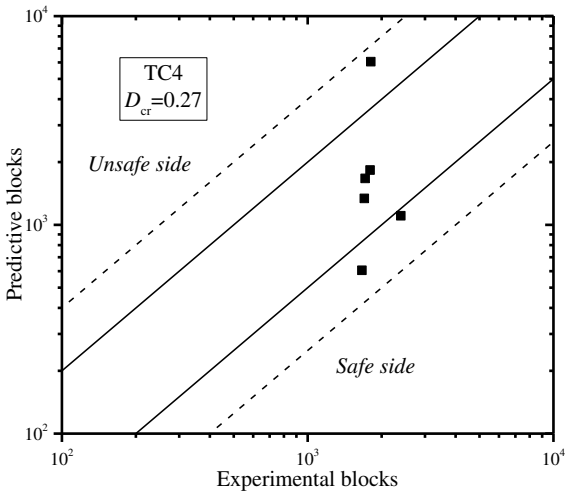
TC4
D_{cr}=0.27
Unsafe side
Safe side
Predictive blocks
Experimental blocks

(*d*)

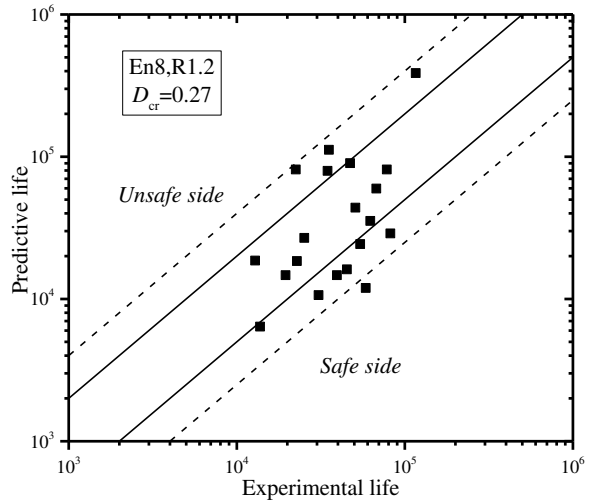
En8,R1.2
D_{cr}=0.27
Unsafe side
Safe side
Predictive life
Experimental life

(*e*)

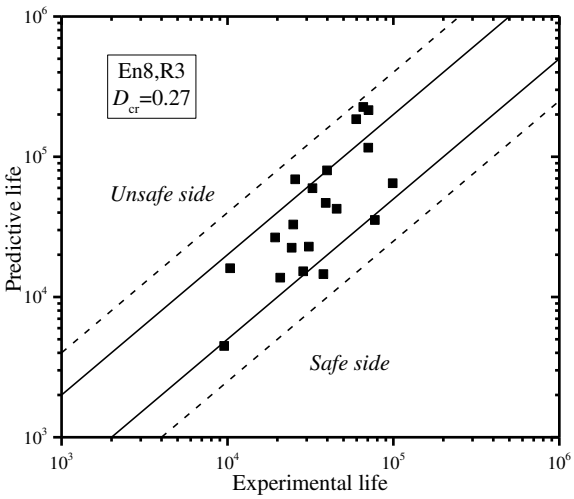
En8,R3
D_{cr}=0.27
Unsafe side
Safe side
Predictive life
Experimental life

(*f*)

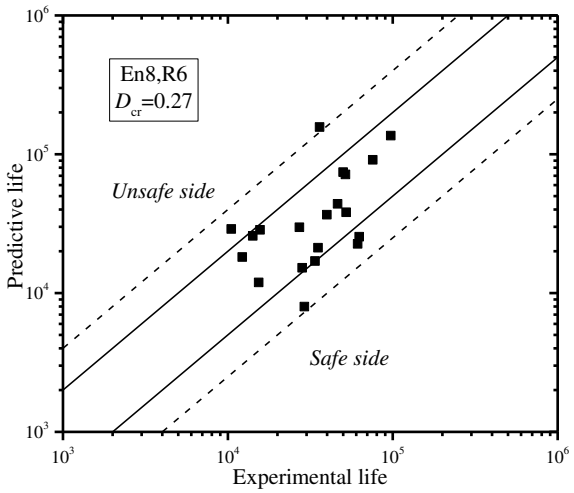
En8,R6
D_{cr}=0.27
Unsafe side
Safe side
Predictive life
Experimental life

(*g*)

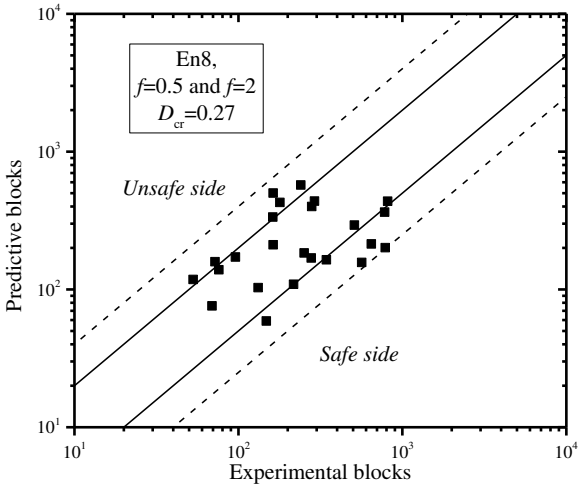
En8,
f=0.5 and f=2
D_{cr}=0.27
Unsafe side
Safe side
Predictive blocks
Experimental blocks

(*h*)

Figure 6 The comparison between experimental life and predicted life for notched specimens

5 Conclusions

(1) The Newton method and the conjugate gradient method are introduced to modify the MVM which is proposed to define the critical plane as the one bearing the maximum variance of resolved shear stress.

(2) Several planes undergo the maximum variance of resolved shear stress. The maximum variance of the normal stress on these potential planes is constructed to define the plane with the maximum normal stress as the critical plane.

(3) A new multiaxial cycle counting method is proposed to count the cycles under complex variable amplitude fatigue loading based on the test conducted by Jordan[54] and Wang *et al*.[26-28].

(4) Nearly two hundred sets of test data of six different kinds of metallic materials are collected to verify the new multiaxial cycle counting method. Experimental results indicate that the methods proposed can accurately evaluate the fatigue life for both plain and notched components under complex variable amplitude cyclic loading.

6 Acknowledgement

The authors acknowledge the support from China Scholarship Council (CSC201906830050) and National Science and Technology Major Project (2017-Ⅵ-0003-0073).

7 References

[1] Han C, Chen X, Kim K. Evaluation of multiaxial fatigue criteria under irregular loading. *Int J Fatigue.* 2002; 24(9): 913–922.

[2] Susmel L. Multiaxial Notch Fatigue: From Nominal to Local Stress-Strain Quantities. Cambridge, UK: Woodhead & CRC;2009.

[3] Fatemi A, Shamsaei N. Multiaxial fatigue: An overview and some approximation models for life estimation. *Int J Fatigue.* 2011;33(8):948–958.

[4] Luo P, Yao WX, Susmel L, Wang YY, Ma XX, A survey on multiaxial fatigue damage

parameters under non-proportional loadings. *Fatigue Fract Eng Mater Struct.* 2017; 40(9):1323–1342.

[5] Luo P, Yao WX, Li P. A notch critical plane approach of multiaxial fatigue life prediction for metallic notched specimens. *Fatigue Fract Eng Mater Struct.* 2019; 42(4): 854–870.

[6] Luo P, Yao WX, Susmel L, Li P. Prediction methods of fatigue critical point for notched components under multiaxial fatigue loading. *Fatigue Fract Eng Mater Struct.*2019; 42(12): 2782–2793.

[7] Fatemi A, Socie DF. A critical plane approach to multiaxial fatigue damage including out-of-phase loading. *Fatigue Fract Eng Mater Struct.* 1988; 11(3) 149–165.

[8] Karolczuk A, Macha E. A review of critical plane orientations in multiaxial fatigue failure criteria of metallic materials. *Int J Fract.* 2005; 134(3–4):267-304.

[9] Socie D. Critical plane approaches for multiaxial fatigue damage assessment. Advances in multiaxial fatigue, ASTM International, 1993.

[10] Crossland B. Effect of large hydrostatic pressures on the torsional fatigue strength of an alloy steel. Proc. Int. Conf. on Fatigue of Metals, 1956;138:12.

[11] Papadopoulos IV. Fatigue polycyclique des métaux: une nouvelle approche. PhD Thesis, Ecole nationale des ponts et chaussées (France), 1987.

[12] Braccesi C, Cianetti F, Lori G, Pioli D. Random multiaxial fatigue: A comparative analysis among selected frequency and time domain fatigue evaluation methods. *Int J Fatigue.* 2015;74:107–118.

[13] Carpinteri A, Spagnoli A, and Vantadori S. A review of multiaxial fatigue criteria for random variable amplitude loads. *Fatigue Fract Eng Mater Struct.* 2017; 40(7):1007–1036.

[14] Dirlik T. Application of computers in fatigue analysis. Ph.D thesis, University of Warwick, 1985.

[15] Bendat JS, Piersol AG. Random data: analysis and measurement procedures. John Wiley & Sons; 2011.

[16] Rice SO. Mathematical analysis of random noise. *Bell System Technical J* 1945;24(1):46–156.

[17] Niesłony A, Růžička M, Papuga J, Hodr A, Balda M, Svoboda J. Fatigue life prediction for broad-band multiaxial loading with various PSD curve shapes. *Int J Fatigue.* 2012; 44:74–88.

[18] Susmel L, Tovo R. Estimating fatigue damage under variable amplitude multiaxial fatigue loading. *Fatigue Fract Eng Mater Struct.* 2011;34(12):1053–1077.

[19] Palmgren A. Die Lebensdauer von Kugellagern. Verfahrenstechnik, Berlin, 1924;68:339-41.

[20] Miner MA. Cumulative damage in fatigue. *J Appl Mech*. 1945;67: A159-A164.

[21] E08 Committee. Practices for Cycle Counting in Fatigue Analysis. ASTM E1049-85, West Conshohocken, PA, 2011.

[22] Matsuishi M, Endo T. Fatigue of metals subjected to varying stress. Japan Society of Mechanical Engineers,1968;.68(2):37–40.

[23] Downing S, Socie D. Simple rainflow counting algorithms. *Int J Fatigue.* 1982;4(1):31–40.

[24] Bannantine JA, Socie DF. A variable amplitude multiaxial fatigue life prediction methods. ICBMFF3, 1990.

[25] Smith KN. A stress-strain function for the fatigue of metals. *J Mater.* 1970;5:767–778.

[26] Wang CH, Brown MW. A path-independent parameter for fatigue under proportional and non-proportional loading. *Fatigue Fract Eng Mater Struct.* 1993 ;16(12):1285–1297.

[27] Wang CH, Brown MW. Life prediction techniques for variable amplitude multiaxial fatigue—Part 1: Theories. *J Eng Mater Technol.* 1996; 118(3):367–370.

[28] Wang CH, Brown MW. Life prediction techniques for variable amplitude multiaxial fatigue—part 2: comparison with experimental results. *J Eng Mater Technol.* 1996; 118(3):371–374.

[29] Carpinteri A, Spagnoli A, Vantadori S. A multiaxial fatigue criterion for random loading. *Fatigue Fract Eng Mater Struct.* 2003; 26(6):515–522.

[30] Carpinteri A, Spagnoli A. Multiaxial high-cycle fatigue criterion for hard metals. *Int J Fatigue.* 2001;23(2):135–145.

[31] Langlais TE, Vogel JH, Chase TR. Multiaxial cycle counting for critical plane methods. *Int J Fatigue*. 2003;25(7):641–647.

[32] Dong P. Wei Z, Hong JK. A path-dependent cycle counting method for variable-amplitude multi-axial loading. *Int J Fatigue*. 2010;32(4):720–734.

[33] Anes V, Reis L, B. Li, M. de Freitas. New cycle counting method for multiaxial fatigue. *Int J Fatigue*.2014; 67:78–94.

[34] Anes V, Reis L, Li B, Fonte M, Freitas M. New approach for analysis of complex multiaxial loading paths. *Int J Fatigue*.2014; 62:21–33.

[35] Portugal I, Olave M, Zurutuza A, López A, Muñiz-Calvente M, Fernández-Canteli A. Methodology to evaluate fatigue damage under multiaxial random loading. *Eng Fract Mech.* 2017;185:114–123.

[36] Papadopoulos IV. Critical Plane Approaches in High-Cycle Fatigue: On the Definition of the Amplitude and Mean Value of the Shear Stress Acting on the Critical Plane. *Fatigue Fract Eng Mater Struct.*1998;21(3):269–285.

[37] Wang XW, Shang DG, Sun YJ, Liu XD. Algorithms for multiaxial cycle counting method and fatigue life prediction based on the weight function critical plane under random loading. *Int J Damage Mech.* 2019; 28(9):1367–1392.

[38] Lu Y. Wu H, Zhong Z. A modified energy-based model for low-cycle fatigue life prediction under multiaxial irregular loading. *Intl J Fatigue*. 2019; 128:105187.

[39] Susmel L, Taylor D. A critical distance/plane method to estimate finite life of notched components under variable amplitude uniaxial/multiaxial fatigue loading. *Int J Fatigue.* 2011; 38:7–24.

[40] Susmel L, Tovo R, Benasciutti D. A novel engineering method based on the critical plane concept to estimate the lifetime of weldments subjected to variable amplitude multiaxial fatigue loading. *Fatigue Fract Eng Mater Struct.* 2009;32(5):441–459.

[41] Susmel L, Taylor D. Estimating lifetime of notched components subjected to variable amplitude fatigue loading according to the elastoplastic Theory of Critical Distances. *J Eng Mater Technol.* 2015; 137(1):011008.

[42] Faruq NZ, Susmel L. Proportional/nonproportional constant/variable amplitude multiaxial notch fatigue: cyclic plasticity, non-zero mean stresses, and critical distance/plane. *Fatigue Fract Eng Mater Struct*. 2019; 42(9):1849-1873.

[43] Susmel L. A simple and efficient numerical algorithm to determine the orientation of the critical plane in multiaxial fatigue problems. *Int J Fatigue.* 2010;32(11):1875–1883.

[44] Scharf LL. Statistical signal processing. Addison-Wesley Reading, MA, 1991.

[45] Dogandzic A, Nehorai A. Generalized multivariate analysis of variance-A unified framework for signal processing in correlated noise. IEEE Signal Processing Magazine 2003;20(5):39–54.

[46] Schwarzenberg-Czerny A. On the advantage of using analysis of variance for period search. Mon Not R Astron Soc 1989;241(2):153–165.

[47] Nash SG. A survey of truncated-Newton methods. *J Computational and Appl Mathematics.* 2000; 124(1):45–59.

[48] Liu Y, Storey C. Efficient generalized conjugate gradient algorithms, part 1: Theory. *J Optim Theory Appl.* 1991; 69(1):129–137.

[49] Morel F. A critical plane approach for life prediction of high cycle fatigue under multiaxial variable amplitude loading. *Int J Fatigue.* 2000;22(2):101-119.

[50] Wang YY, Susmel L. Critical plane approach to multiaxial variable amplitude fatigue loading. *Frattura ed Integrità Strutturale*. 2015;9(33):345–356,.

[51] Susmel L, Lazzarin P. A bi-parametric Wöhler curve for high cycle multiaxial fatigue assessment. *Fatigue Fract Eng Mater Struct.* 2002; 25(1):63–78.

[52] Lazzarin P, Susmel L. A stress-based method to predict lifetime under multiaxial fatigue loadings. *Fatigue Fract Eng Mater Struct.* 2003; 26(12):1171–1187.

[53] Susmel L. Multiaxial fatigue limits and material sensitivity to non-zero mean stresses normal to the critical planes. *Fatigue Fract Eng Mater Struct.* 2008; 31(3–4):295–309.

[54] Jordan E, Brown M, Miller K. Fatigue under severe nonproportional loading. Multiaxial Fatigue, K. Miller and M. Brown, Eds. 100 Barr Harbor Drive, PO Box C700, West Conshohocken, PA 19428-2959: ASTM International, 1985:569-569–17.

[55] Xia TX, Yao WX. Comparative research on the accumulative damage rules under multiaxial block loading spectrum for 2024-T4 aluminum alloy. *Int J Fatigue.* 2012; 48(257–265).

[56] Lasserre S, Froustey C. Multiaxial fatigue of steel—testing out of phase and in blocks: validity and applicability of some criteria. *Int J Fatigue.* 1992;14(2):113–120.

[57] Bernasconi A, Foletti S, Papadopoulos IV. A study on combined torsion and axial load fatigue limit tests with stresses of different frequencies. *Int J Fatigue.* 2008;30(8):1430–1440.

[58] Wu ZR. Research on multiaxial fatigue life prediction method for Titanium alloy. Ph.D. thesis. Nanjing: Nanjing University of Aeronautics and Astronautics, 2014.(In chinese)

[59] Davoli P, Bernasconi A, Filippini M, Foletti S, and Papadopoulos IV. Independence of the torsional fatigue limit upon a mean shear stress. *Int J Fatigue.* 2003: 25(6,):471–480.

[60] Lagoda T, Sonsino CM. Comparison of different methods for presenting variable amplitude loading fatigue results. Materialwissenschaft und Werkstofftechnik 2004;35(1):13–20.

[61] Sonsino CM. Fatigue testing under variable amplitude loading. *Int J Fatigue.* 2006;29(6):1080–1089.

[62] Sonsino CM. Limitations in the use of RMS values and equivalent stresses in variable amplitude loading. *Int J Fatigue.* 1989; 11(3):142–152.

Appendix 1 The Newton method and the conjugate gradient method

Eq. (15) is a ternary function which can be rewritten as follows:

$$\mathrm{Var}\left[\tau_q(t)\right] = f(\alpha,\phi,\theta) \tag{A1.1}$$

The illustrations of the Newton method and the conjugate gradient method to iteratively search the local maximum value are shown in Figure A1.1 and Figure A1.2 respectively. The Newton method uses the Hessian matrix which consists of the second-order partial derivatives of the multivariate function. The expression of the Hessian matrix in Eq. (A1.1) is:

$$\boldsymbol{G} = \begin{bmatrix} \dfrac{\partial^2 f}{\partial \varphi^2} & \dfrac{\partial^2 f}{\partial \varphi \partial \theta} & \dfrac{\partial^2 f}{\partial \varphi \partial \alpha} \\ \dfrac{\partial^2 f}{\partial \theta \partial \varphi} & \dfrac{\partial^2 f}{\partial \theta^2} & \dfrac{\partial^2 f}{\partial \theta \partial \alpha} \\ \dfrac{\partial^2 f}{\partial \alpha \partial \varphi} & \dfrac{\partial^2 f}{\partial \alpha \partial \theta} & \dfrac{\partial^2 f}{\partial \alpha^2} \end{bmatrix} \tag{A1.2}$$

In essence, the Newton method is second-order convergent while the gradient ascent method is first-order convergent. So, the convergent rate of the Newton method is very fast due to the second-order partial derivative, but it is not easy to calculate the inverse matrix $\boldsymbol{G}^{-1}$ of the Hessian matrix $\boldsymbol{G}$ in some cases. The conjugate gradient method is a typical conjugate direction method. Each searching direction is mutually conjugate, and these search directions are only the combination of the gradient direction and the searching direction of the last iteration. Therefore, the storage is small and the calculation is convenient and easy. The k is a variable in Figure A1.1 and Figure A1.2, and we can know that the function g(k) is a one-variable function. The function g(k) reaches the maximum value when k is equal to k_{n}. ε is a small value that controls the accuracy of the critical plane in Figure A1.1 and Figure A1.2. The first step of Figure A1.1 and Figure A1.2 is to get different initial values where the local maximum value can be searched. There are many local maximums, but some of them are global maximums. In other words, several planes bear the maximum variance of the resolved shear stress. The plane with the maximum normal stress is the critical plane among these potential planes.

The process of Newton's method and conjugate gradient method can be easily achieved through the programming in the software Matlab. The accuracy of the numerical solution depends on the value ε. The tension-torsional fully reversed cyclic loadings are used as examples to further explain these algorithms. The computing times of three algorithms are summarized in Figure A1.3 where the first number is the ratio between the normal stress σ_x and the shear stress τ_{xy} and the second number is the phase in the abscissa. For example, '1-45° ' means that the ratio between the normal stress σ_x and the shear stress τ_{xy} is 1 and the phase is 45° . The mean values of the computing time under these cyclic loading to determine the critical plane are listed in Table where the conjugate gradient method is the fastest one to search the critical plane.

Table A1.1 The mean values of the computing time (unit: s)

Loading paths	The algorithm in Ref. [43]	Conjugate gradient method	Newton method
Proportional loading	520.0	11.9	95.7
Non-proportional loading	713.9	12.3	111.8

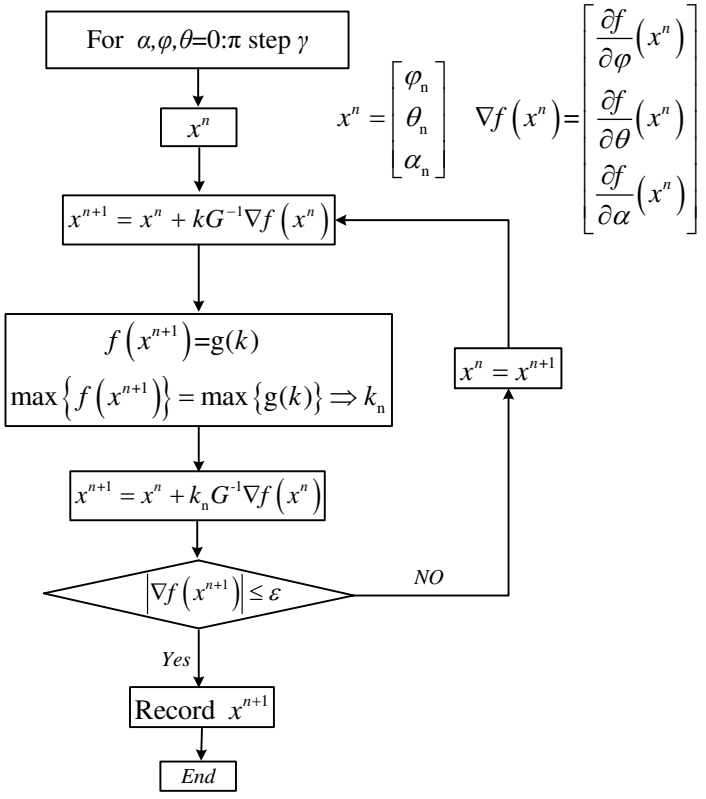

Figure A1.1 The illustration of the Newton method

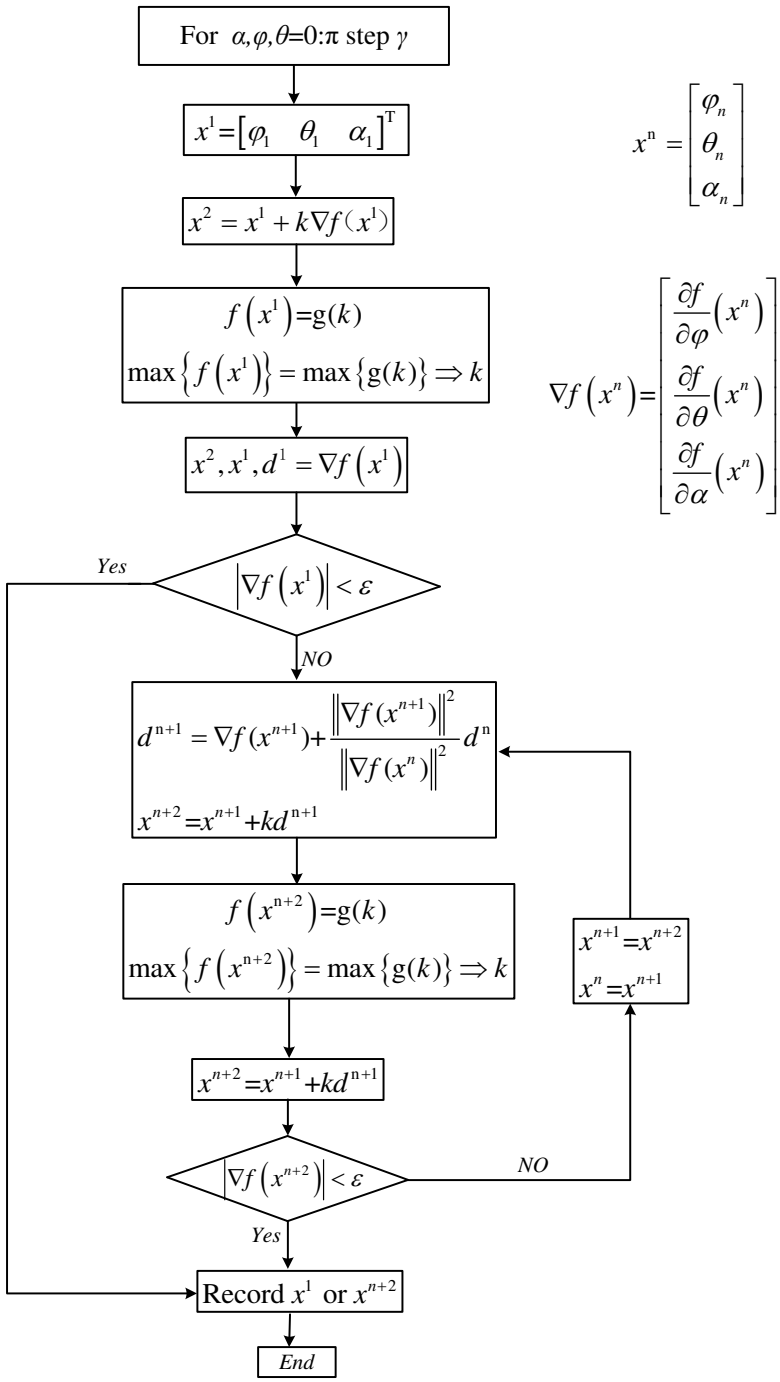

Figure A1.2 The illustration of the conjugate gradient method

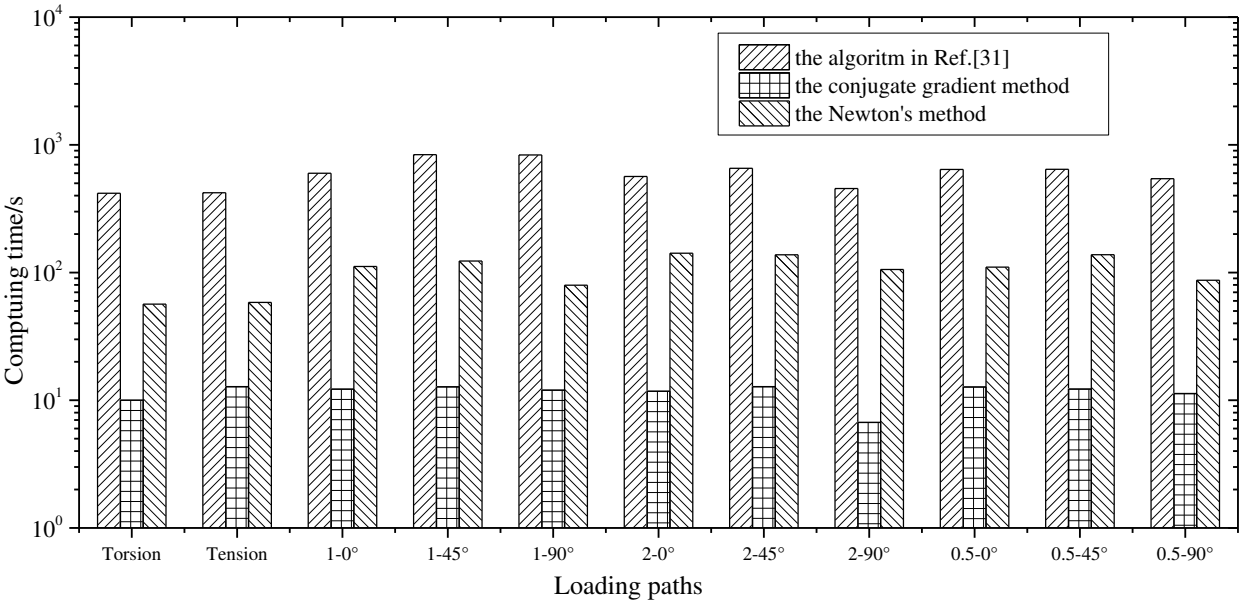

Figure A1.3 The computing times of three algorithms

Note: '1-45° ' in abscissa means that the ratio between the normal stress σ_x and the shear stress τ_{xy} is 1 and the phase is 45° for tension-torsional cyclic loading.

Appendix 2 Multiaxial variable fatigue loading history

2.1 Multiaxial variable fatigue loading history of 2020-T4

Table A2.1 Multiaxial constant amplitude fatigue loading

No.	Loading type	σ_a (MPa)	τ_a (MPa)
A	Uniaxial tension-compression	250	0
B		350	0
C	Pure torsion	0	144.3
D		0	167
E	Proportional	158.1	111.8
F		177	102.2
G		248	143
H	30° Proportional	158	120
I	45° Proportional	158	125
J		248	143.2
K	60° Proportional	158	132
L	90° Proportional	177	102.2
M		158.1	139.1
N		244	157.2
O		250	144.3
P		250	125

Table A2.2 Multiaxial variable amplitude fatigue loading

Multiaxial variable amplitude fatigue loading	Composition of spectrum
VL1_TC4	D-O-I-A
VL2_TC4	A-P-H-E-M-K-O-I
VL3_TC4	D-L-J-G-B-N-F-H
VL4_TC4	O-D-G-M-H-F-G-H-O-H-M-N-J-E-K-F-G-G-K-A-F-N-B-B -B-B-B-I-F-J-P-O-A-B-B-B-B-B-B-B-B-B-B-N-O-B-B-B
VL5_TC4	L-C-A-C-I-G-C-D-B-N-D-P-B-B-G-O-L-I-P-B-D-C-M-P-D -K-L-I-A-L-C-H-M-P-D-A-H-C-I-J-K-H-D-E-F-D-L-O-G-I
VL6_TC4	O-M-B-B-B-B-B-F-G-E-L-A-M-I-I-B-B-B-B-B-I-H-A-P -H-G-P-I-B-B-B-B-B-J-D-O-P-P-H-O-M-A-H-G-D-K-J-O-L-A
VL7_TC4	E-B-B-B-B-B-E-P-B-B-B-B-B-G-D-K-N-N-F-L-O-G-M-A- P-O-L-E-F-G-I-D-B-B-B-B-B-H-L-J-O-H-M-O-P-D-I-B-B-B

Note: The multiaxial variable amplitude fatigue loadings of 2020-T4 are based on the multiaxial constant amplitude fatigue loadings in Table A2.1

2.2 Multiaxial variable fatigue loading history of XC18

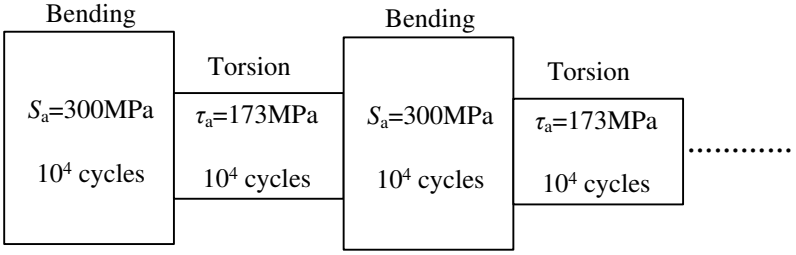

Figure A2.1 Multiaxial variable fatigue loading No. VL1_XC18

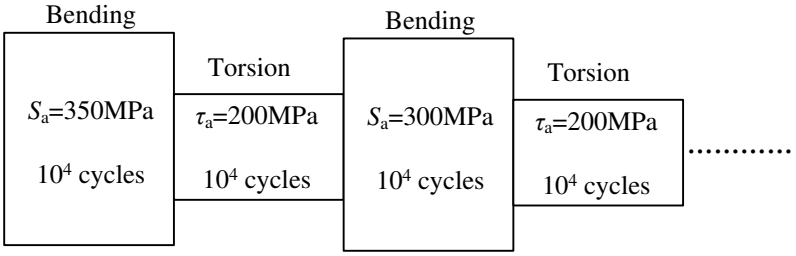

Figure A2.2 Multiaxial variable fatigue loading No. VL2_XC18

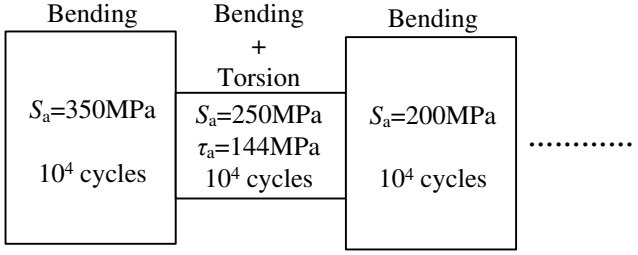

Figure A2.3 Multiaxial variable fatigue loading No. VL3_XC18

2.3 Multiaxial variable fatigue loading history of 39NiCrMo3

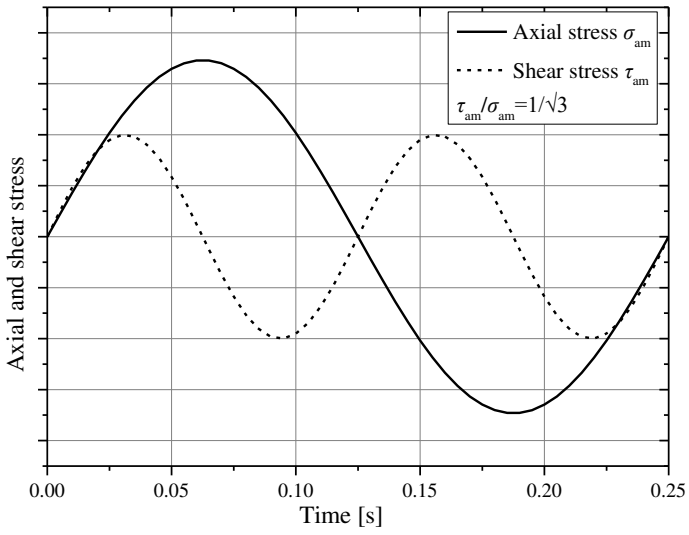

Figure A2.4 Multiaxial variable fatigue loading No. VL1_39NiCrMo3

2.4 Multiaxial variable fatigue loading history of C40

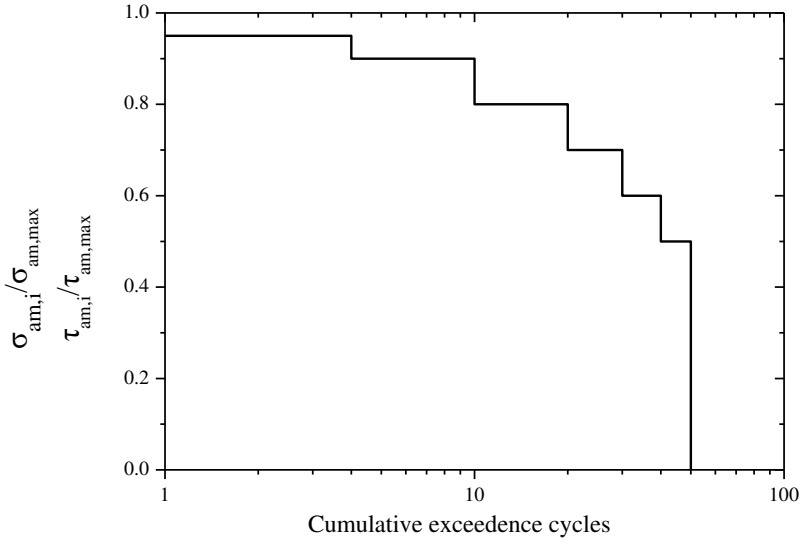

Figure A2.5 Multiaxial variable fatigue loading No. VL1_C40

2.5 Multiaxial variable fatigue loading history of TC4

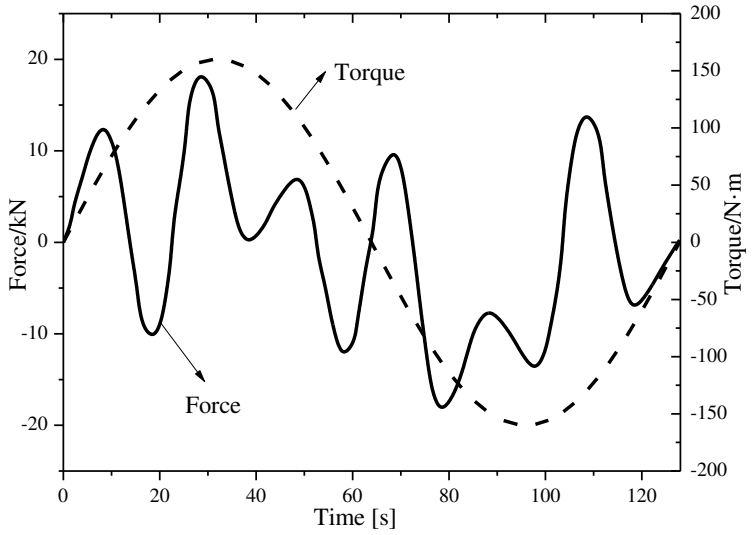

Figure A2.6 Multiaxial variable fatigue loading No. VL1_TC4

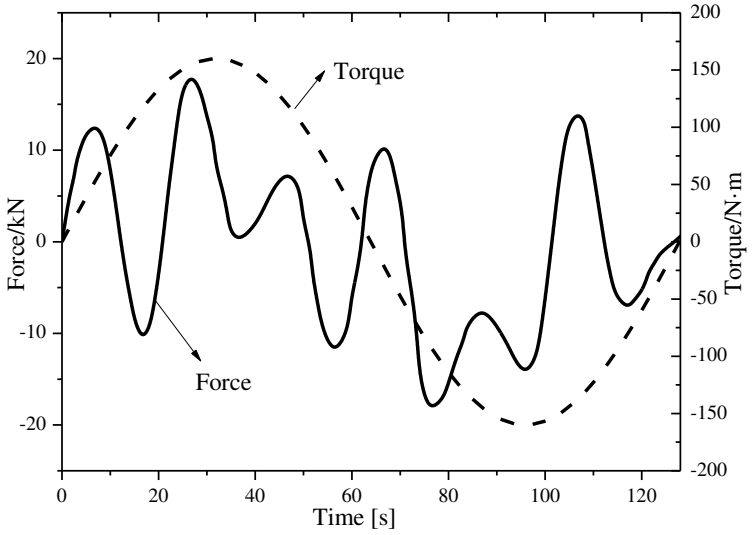

Figure A2.7 Multiaxial variable fatigue loading No. VL2_TC4

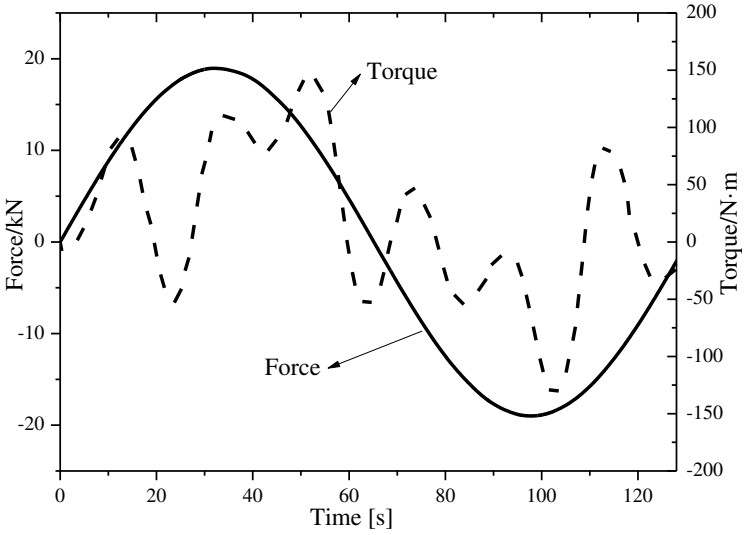

Figure A2.8 Multiaxial variable fatigue loading No. VL3_TC4

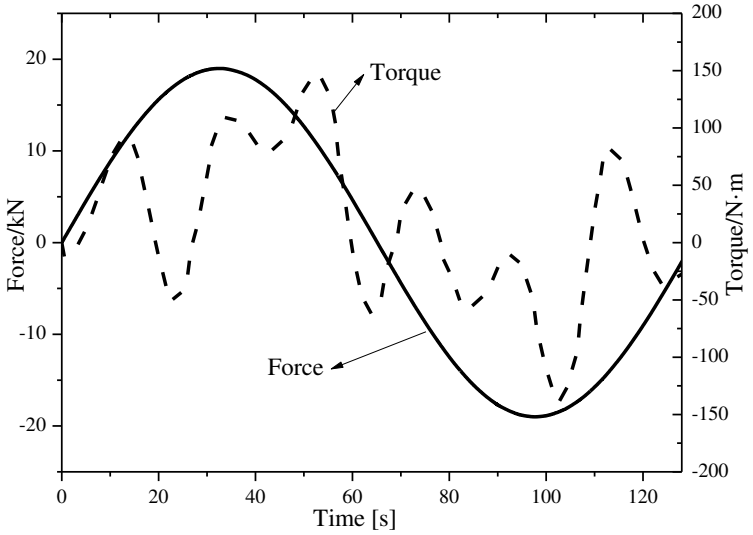

Figure A2.9 Multiaxial variable fatigue loading No. VL4_TC4

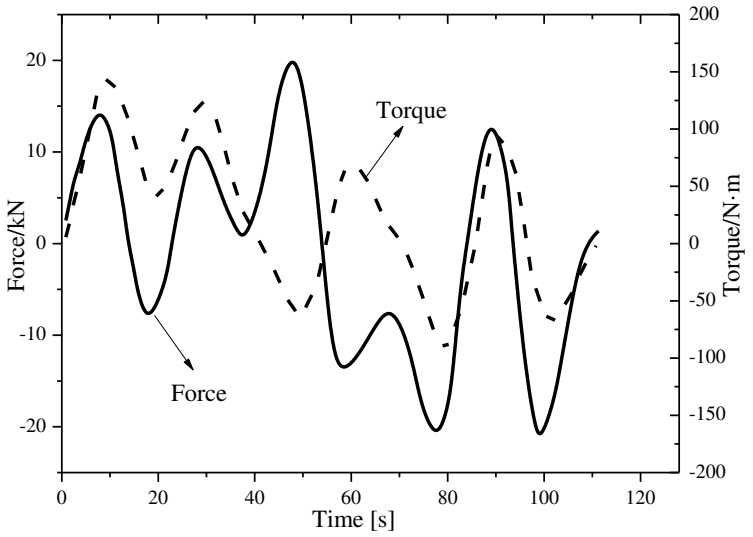

Figure A2.10 Multiaxial variable fatigue loading No. VL5_TC4

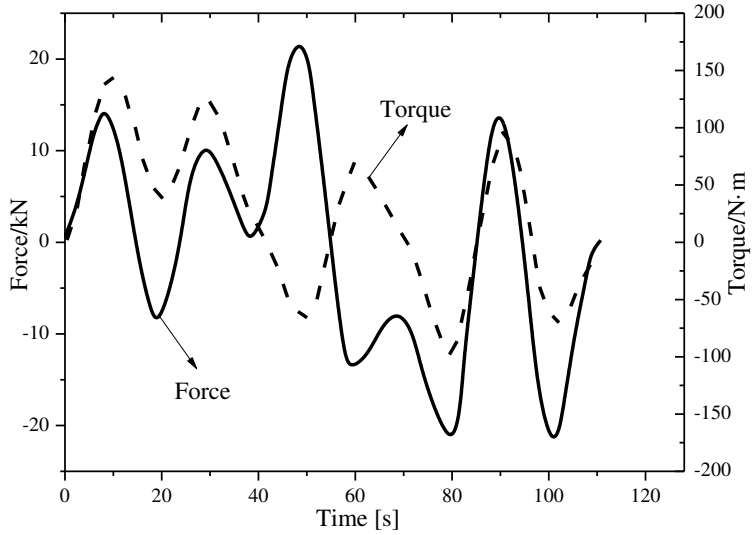

Figure A2.11 Multiaxial variable fatigue loading No. VL6_TC4

2.6 Multiaxial variable fatigue loading history of En8

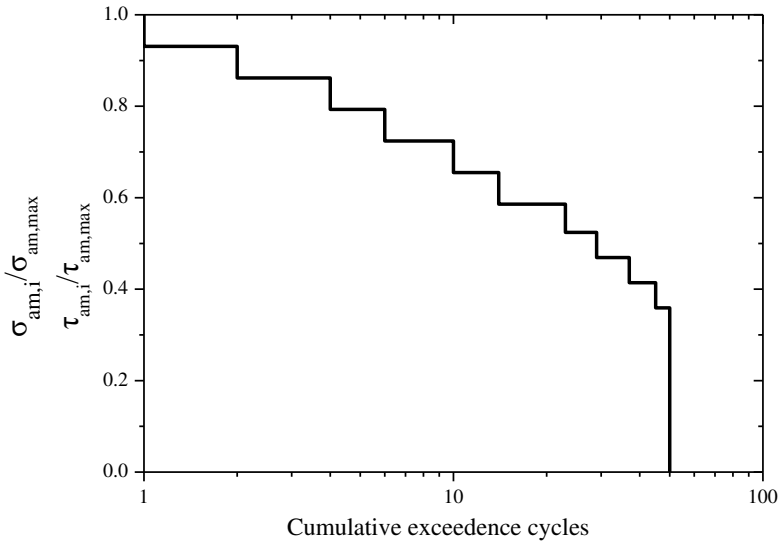

Figure A2.12 Multiaxial variable fatigue loading No. VL1_En8